Crystal Phases and Thermal Stability of Co-Evaporated $\mathrm{CsPbX_3}$ $(\mathrm{X = I, Br})$ Thin Films

Thomas Burwig, Wolfgang Fränzel, and Paul Pistor[*]

Faculty of Natural Sciences II, Martin Luther University Halle-Wittenberg, Halle (Saale)

E-mail: paul.pistor@physik.uni-halle.de

Abstract

In this work we present the growth, phase transitions and thermal decomposition of $CsPbX_3$ ($X = I, Br$) thin films monitored by *in situ* X-ray diffraction. The perovskite films are prepared in vacuum via co-evaporation of PbX_2 and CsX ($X = I, Br$) onto glass substrates. *In-situ* X-ray diffraction allows the observation of phase transitions and decomposition while the samples are heated with a linear temperature ramp. Our experiments reveal the decomposition route for the $CsPbX_3$ perovskites in high vacuum, with a much higher stability than their hybrid organic-inorganic $MAPbX_3$ counterparts. We also observed the response of a black $CsPbI_3$ thin film to exposure to ambient air at room temperature using the same XRD system. Exposing the black $CsPbI_3$ to ambient air leads to the formation of yellow orthorhombic δ-$CsPbI_3$, whose crystal structure could be identified by its X-ray diffraction pattern. Additionally, the linear coefficients of expansion are determined for δ-$CsPbI_3$ and the (020)-orientation of $CsPbBr_3$.

TOC GRAPHIC
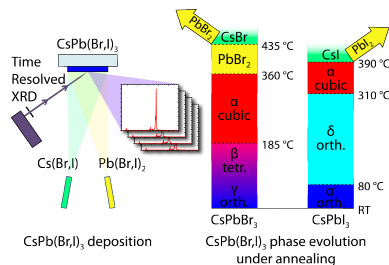
Introduction

Within the last years organo-metal halide perovskites have shown promising results as absorber materials for photovoltaic cells. Most of the current day research focuses on perovskites with the general sum formula $APbX_3$, with X being a halide - mostly Cl, Br or I - and A being an organic cation like methylammonium (MA) or formamidinium (FA).

Some of the greater challenges of current perovskite technologies are concerns about thermal stability[1,2] as well as a high susceptibility to water induced damage.[3–5] There is a growing body of evidence that suggests that the organic A component only plays a minor role for perovskites in regards to their use case as photovoltaic absorbers,[6–8] with charge carrier mobility and lifetime mostly determined by the PbX_3 framework.[9] In more recent works, perovskites, where the organic A cation is partially or fully substituted by the inorganic Cs, have seen rising attention.[6,7,9–11] The motivation behind this substitution is the expectation to increase the stability of the resulting perovskite.[2,6,12]

$CsPbBr_3$ has been reported by Hirotsu et al. to exist in an orthorhombic structure (Pbnm, $a = 8.207\,\text{Å}, b = 8.255\,\text{Å}, c = 11.759\,\text{Å}$) at room temperature, with a transition to a tetragonal structure (P4/mbm, $a = 8.259\,\text{Å}, b = 5.897\,\text{Å}$) above $88\,°\text{C}$ and to a cubic structure (Pm-3m, $a = 5.874\,\text{Å}$) above $130\,°\text{C}$.[13] The XRD peak positions that result from these crystal structures will be used to identify the different $CsPbBr_3$-phases and peaks. In accordance with established convention, the cubic phase of this perovskite will henceforth be referred to as α, the tetragonal phase as β and the orthorhombic phase as γ. The band gap energy of pure $CsPbBr_3$ is $2.25\,\text{eV}$[14] and thus it is too high for efficient absorption of photons within the visible spectrum. However, incorporating I to subsitute the Br will decrease its band gap to as low as $1.73\,\text{eV}$.[15]

At room temperature, $CsPbI_3$ can exist in a black, meta-stable α-phase that has often been assumed to be cubic and a yellow, orthorhombic, non-perovskite δ-phase.[16] The black α-phase has a band gap of $1.73\,\text{eV}$[15] which renders it suitable for the use as a photovoltaic absorber. This band gap makes it especially useful as a top cell of a silicon tandem solar cell. The yellow δ-phase has a band gap of $3.01\,\text{eV}$,[17] which is far too large for efficiently absorbing visible sunlight. The cubic α-phase, however, has been reported to only be stable for temperatures above $300\,°\text{C}$.[8,16] The crystal structure of the black α perovskite phase at room temperature has been identified as orthorhombic instead of cubic by some researchers.[18] Since this phase therefore differs from the black α-phase at high temperatures, the room

temperature phase will henceforth be referred to as α'. To identify the phases and the peaks of the CsPbI$_3$, the works of Trots et al. and Lai et al. have been used.[18,19] The α'-phase is unstable under ambient air and, if exposed to it, will convert to the δ-phase.[8,16] Some researchers expect the influx of water molecules into the perovskite matrix to be the driving force behind this phase transition.[12] There have been different successful approaches for increasing the stability of the black CsPbI$_3$ perovskite at room temperature. Some examples include the solution processing of CsPbI$_3$ by using alkyl phosphinic acid as a solvent,[20] incorporating FA into the A position[21] or incorporating Br into the X position.[11]

In this work we present the growth and thermal decomposition of CsPbBr$_3$ and CsPbI$_3$ as well as the response of α'-CsPbI$_3$ to ambient air, for the first time monitored by an *in situ* XRD system. This allows for an easy correlation of the development of the XRD peaks to the temperature and to the applied atmosphere. One major benefit of our approach is the possibility to analyse the crystal phases without the need for interrupting the process or breaking the vacuum, and therefore the avoidance of air exposure. Furthermore, the setup allows to easily the determine of linear thermal expansion coefficients, which has been carried out for the (020)-plain of the orthorhombic CsPbBr$_3$ and for the three lattice constants of δ-CsPbI$_3$.

Results and Discussion

The results of the growth and decomposition experiments are shown in figure 1 and 2. Experimental details on the co-evaporation process and *in situ* XRD measurement setup can be found in the supporting information.

In the first experiment, (figure 1), CsBr and PbBr$_2$ are evaporated simultanously from two different evaporation sources. After the sources had reached their target temperatures, the source shutters were opened (marked in the graph with a red arrow). Almost immediately, the deposition of a crystalline perovskite thin film starts and can be monitored via XRD

4

with an increasing signal intensity.

In order to observe the formation and decomposition of the films, the integrated peak intensity of the most intensive peaks is calculated and normalized to one. This normalized, integrated peak area of peak (hkl) and component i will henceforth be referred to as $A_i^{(hkl)}$ and is plotted in the topmost graphs of figures 1 and 2. Below these graphs a colormap is shown, depicting the data of the XRD scans over the course of the experiment. The bottom graph shows the respective temperatures of the substrate and the evaporation sources.

Details on the substrate preparation, the setup and experimental procedure can be found in the supporting information.

During the growth of the $CsPbBr_3$ (Fig. 1 (a)), the most intensive peak of the grown film was the (020) peak at $21.44\,°$ with a FWHM of $0.15\,°$. Additional peaks corresponding to (220), (114), (132), (004), (120) and (002) were also found, named in order of the respective peaks' intensity. An XRD scan of the final $CsPbBr_3$ film can be found in figure 3 (a). All peaks can be assigned to the orthorhombic γ-$CsPbBr_3$, no secondary phases where identified by XRD. The peaks were indexed according to the γ-phase. Despite possible phase transitions to higher symmetry perovskite phases, the indices were retained at higher temperatures for easier readability. Laser light scattering (LLS) indicated a film thickness of roughly $1,200\,nm$. The perovskites growth rate was around $0.2\,nm\,s^{-1}$.

We were not able to detect the phase transition from γ- to β-$CsPbBr_3$ predicted at $80\,°C$,[13] mainly because the γ- and β-phase have many XRD peaks in common and preferential orientations might inhibit the detection of some lattice reflections. The transition from the β- to the α-phase, however, can be asserted by the decline of the (210) peak as visible by $A_{CsPbBr_3}^{(210)}$. Due to the low intensity of the (210) peak, however, $A_{CsPbBr_3}^{(210)}$ has a low signal to noise ratio and the onset of the decline is difficult to determine. The (210) and the (004) peak have fully disappeared at $185\,°C$, which indicates that pure α-$CsPbBr_3$ is present within section II. This phase transition is also marked by a rapid decline of $A_{CsPbBr_3}^{(020)}$ and the emergence of $PbBr_2$ within the film, as indicated by a rapid rise of $A_{PbBr2}^{(200)}$. One
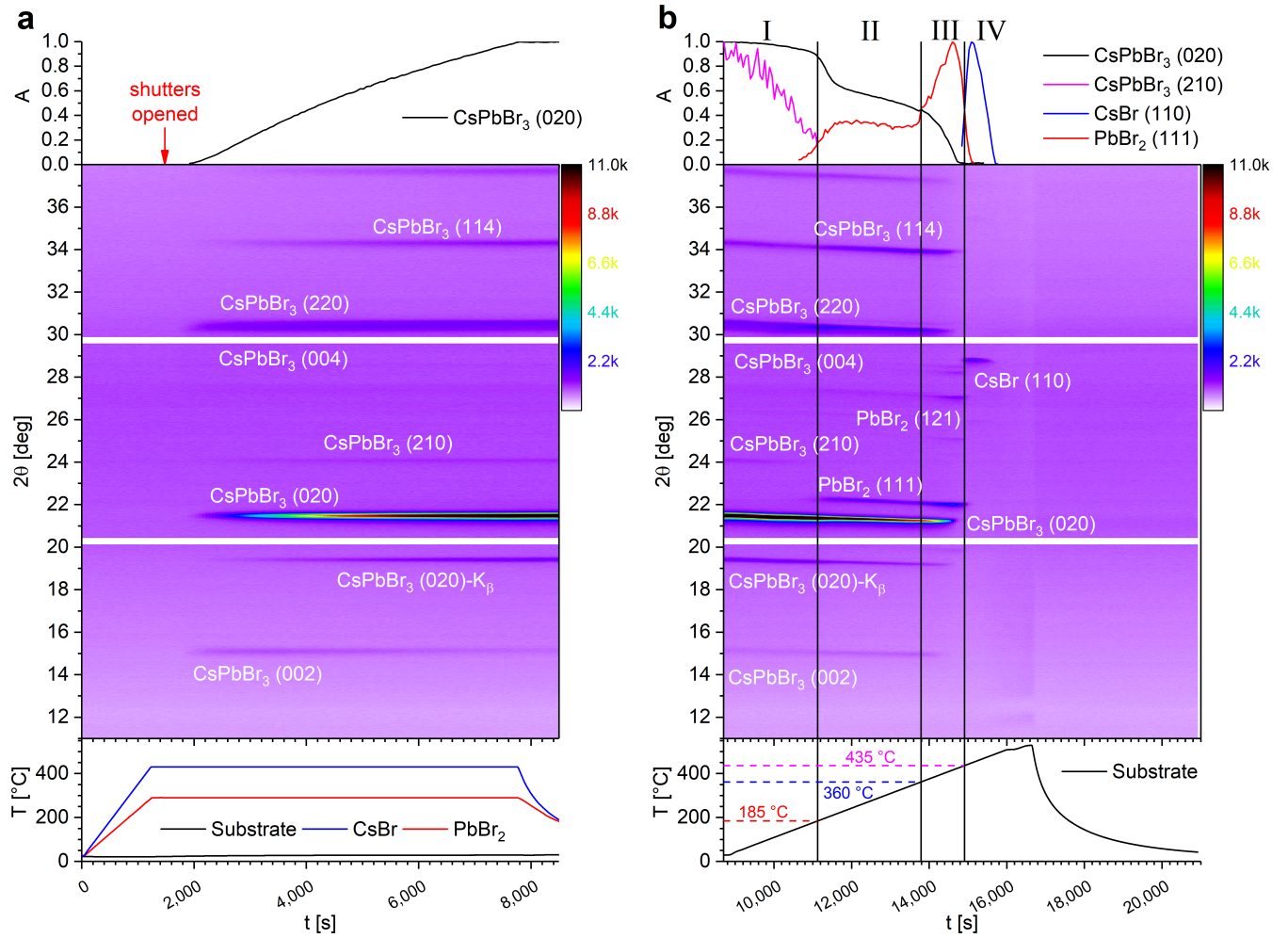
Figure 1: Growth and decomposition of a CsPbBr₃ film. The uppermost chart shows the normalized integrated peak intensity A, the middle chart shows a colour-map-representation of the XRD scans taken during the experiment and the bottom chart shows the temperature of the evaporation sources and of the substrate. (a) shows the growth of the perovskite thin film, (b) its annealing and decomposition. The peaks are indexed according to the γ-phase of CsPbBr₃ at room temperature and this naming is retained throughout the experiment.

possible interpretation of this is that the perovskite is partly decomposing into crystalline $PbBr_2$ while the CsBr remains in an amorphous state which is not detected by XRD. The (020) $CsPbBr_3$ peak further diminishes slowly until section III, which starts at $360\,°C$, where $A_{PbBr_2}^{(200)}$ rapidly increases and $A_{CsPbBr_3}^{(020)}$ decreases. $A_{PbBr2}^{(020)}$ reaches its maximum at around the same time that $A_{CsPbBr_3}^{(020)}$ reaches its minimum, indicating a complete decomposition of the perovskite. Shortly afterwards, in section IV, beginning at $435\,°C$, a (110) CsBr peak appears and the $PbBr_2$ evaporates off of the substrate, leaving behind only the CsBr, which is then fully evaporated soon after. It is notable that the CsBr peak only appears for temperatures $> 435\,°C$, when the $PbBr_2$ has left the film. As noted before, it is possible that the CsBr forms an amorphous phase that only crystallizes at high temperatures when all other components have left the substrate. Another explanation would that a significant portion of the $PbBr_2$ covered the substrates surface, absorbing the majority of the X-ray photons from below. Only when this $PbBr_2$ vanished from the surface did the CsBr become visible to XRD. To estimate whether this is a realistic proposition, the absorption of $PbBr_2$ has been calculated for a film that has the full films' thickness directly after the growth of $1,200\,nm$. The result is an absorption of roughly $12\,\%$, which renders the aforementioned explanation implausible. We therefore tentatively explain the late appearance of CsBr peaks with an amorphous phase being present at lower temperatures.

The $CsPbI_3$ experiment is depicted in figure 2. The XRD peaks of the grown $CsPbI_3$ film indicate the growth of a black α'-$CsPbI_3$ film (Fig. 2 (a)). The XRD pattern of the grown film is shown in figure 3 (e). The position and intensity of these XRD peaks coincide with the results of Lai et al.,[18] and the (hkl) indices have been assigned according to their findings. The two most intensive peaks where the (004) peak at $28.92\,°$ with a FWHM of 0.18 and the (220) peak at $28.58\,°$ with a FWHM of 0.17. The (002) peak was also present. The split (004)-(220) double peak indicates that the black α'-$CsPbI_3$ indeed exists in an orthorhombic structure and not, as is often assumed, in a cubic structure. According to the laser light scattering the layer had a thickness of about $700\,nm$ and was grown at a rate of
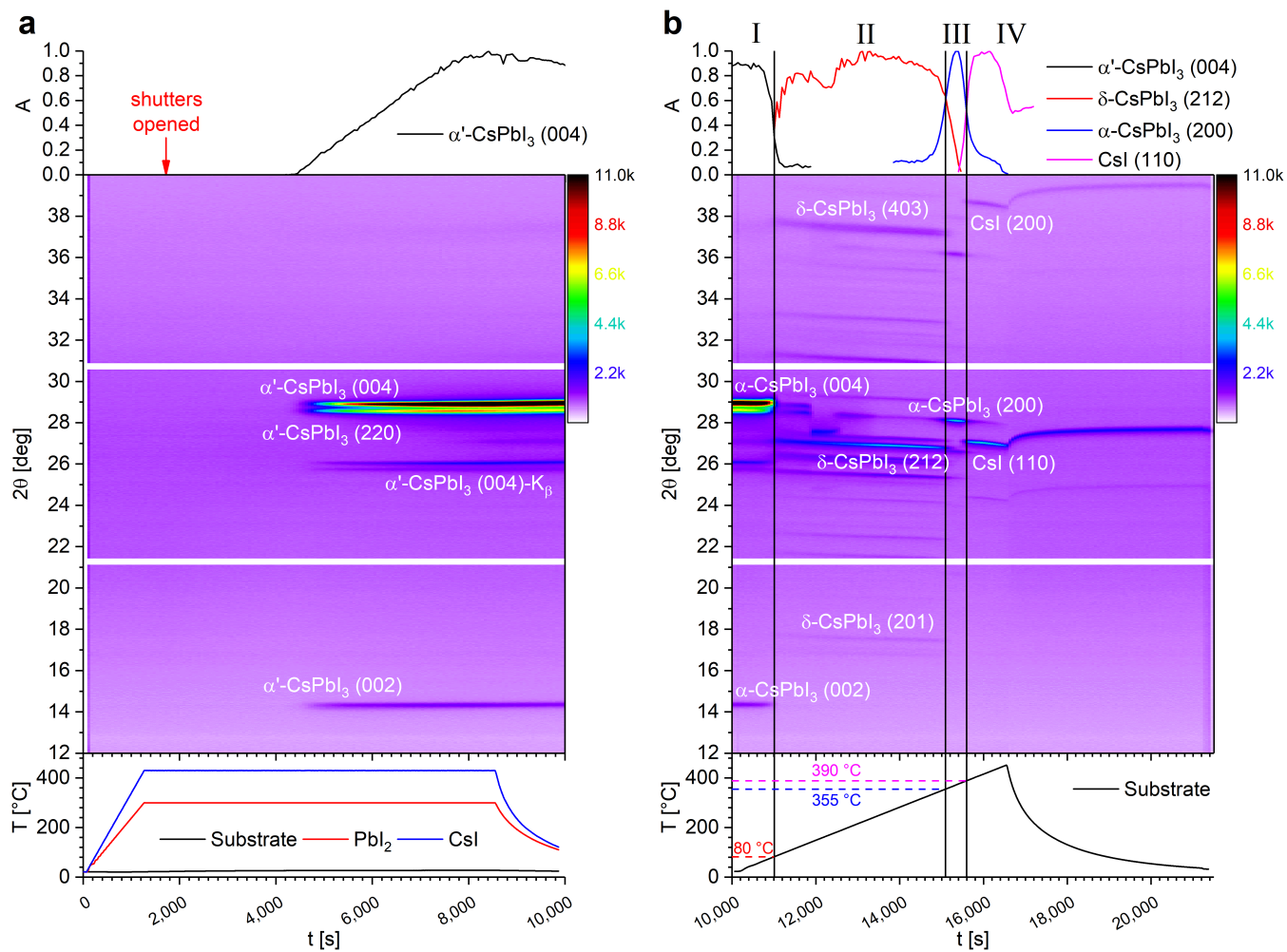
Figure 2: Growth and decomposition of a CsPbI$_3$ film. The uppermost chart shows the normalized integrated peak intensity A, the middle chart shows a colour-map-representation of the XRD-scans taken during the experiment and the bottom chart shows the temperatures of the evaporation sources and of the substrate. (a) shows the growth, (b) the annealing and decomposition of the CsPbI$_3$ perovskite thin film.

8

$0.1\,\mathrm{nm\,s^{-1}}$.

There exists a notable difference to the growth of $CsPbBr_3$: The first XRD peaks appear only more than 2000 s after the opening of the source shutter, while the LLS indicated a continuous thin film deposition during this time. We interpret this as an initial amorphous growth phase of the α'-$CsPbI_3$ perovskite film, which only crystallizes and becomes detectable with XRD at a later time.

One notable feature of the $CsPbI_3$ decomposition experiment depicted in figure 2 (b) is the conversion of the black α'-perovskite to the yellow δ-phase at roughly $80\,^\circ\mathrm{C}$, which is marked in figure 2 as the transition from section I to section II. During this transition $A^{(004)}_{\alpha'\text{-}CsPbI_3}$ quickly decreases and the (212) peak of the δ-phase emerges. This is in good agreement with the findings of Chen et al., who reported this phase transition at $80\,^\circ\mathrm{C}$.[11] In contrast to the $CsPbBr_3$, which is cubic above $130\,^\circ\mathrm{C}$,[13,22] the $CsPbI_3$ will convert from the yellow orthorhombic δ-phase to the cubic α-phase at much higher temperatures. The point at which $A^{(212)}_{\delta\text{-}CsPbI_3}$ drops to $90\,\%$ of its maximum value can be interpreted as the onset of this phase transition and this point is reached at roughly $310\,^\circ\mathrm{C}$. $A^{(212)}_{\delta\text{-}CsPbI_3}$ and $A^{(200)}_{\alpha\text{-}CsPbI_3}$ intersect when both reach a value of roughly 0.6 ($355\,^\circ\mathrm{C}$). It can be asserted that at this point the majority of the δ-$CsPbI_3$ has been converted to α-$CsPbI_3$. At $365\,^\circ\mathrm{C}$ $A^{(200)}_{\alpha\text{-}CsPbI_3}$ reaches its maximum while the δ-$CsPbI_3$ peaks completely disappear. After the complete conversion the intensity of the main α-$CsPbI_3$ peak declines quickly and CsI starts to get visible in the XRD scans. Starting at section IV at $390\,^\circ\mathrm{C}$ $A^{(110)}_{CsI}$ surpasses $A^{(200)}_{\alpha\text{-}CsPbI_3}$ and at $440\,^\circ\mathrm{C}$ the main peak of the α-$CsPbI_3$ completely vanishes. The CsI starts evaporating at roughly $430\,^\circ\mathrm{C}$.

The observed behaviour illustrates one notable difference that the decomposition routes of the all inorganic Cs based perovskites show compared to organic-inorganic $MAPbX_3$ perovskites. The MA based perovskites decompose in such a way that the MA halide component leaves the film first, leaving behind the lead halide.[23–25] With the Cs based perovskites this relation is reversed: The respective lead halide leaves the film first and the Cs halide re-

mains. This indicates that the thermal stability of Cs based perovskites is limited by the lead halide instead of the MA halide component. This provides an explanation for the higher thermal stability that is observed with Cs based perovskites. When we annealed MAPbX$_3$ perovskites under identical conditions, we found for MAPbI$_3$ a decomposition temperature of 230 °C[25] compared to the 360 °C of CsPbI$_3$. The Br analogue MAPbBr$_3$ was shown to decompose at 250 °C[25] compared to CsPbBr$_3$ with its decomposition at 390 °C.
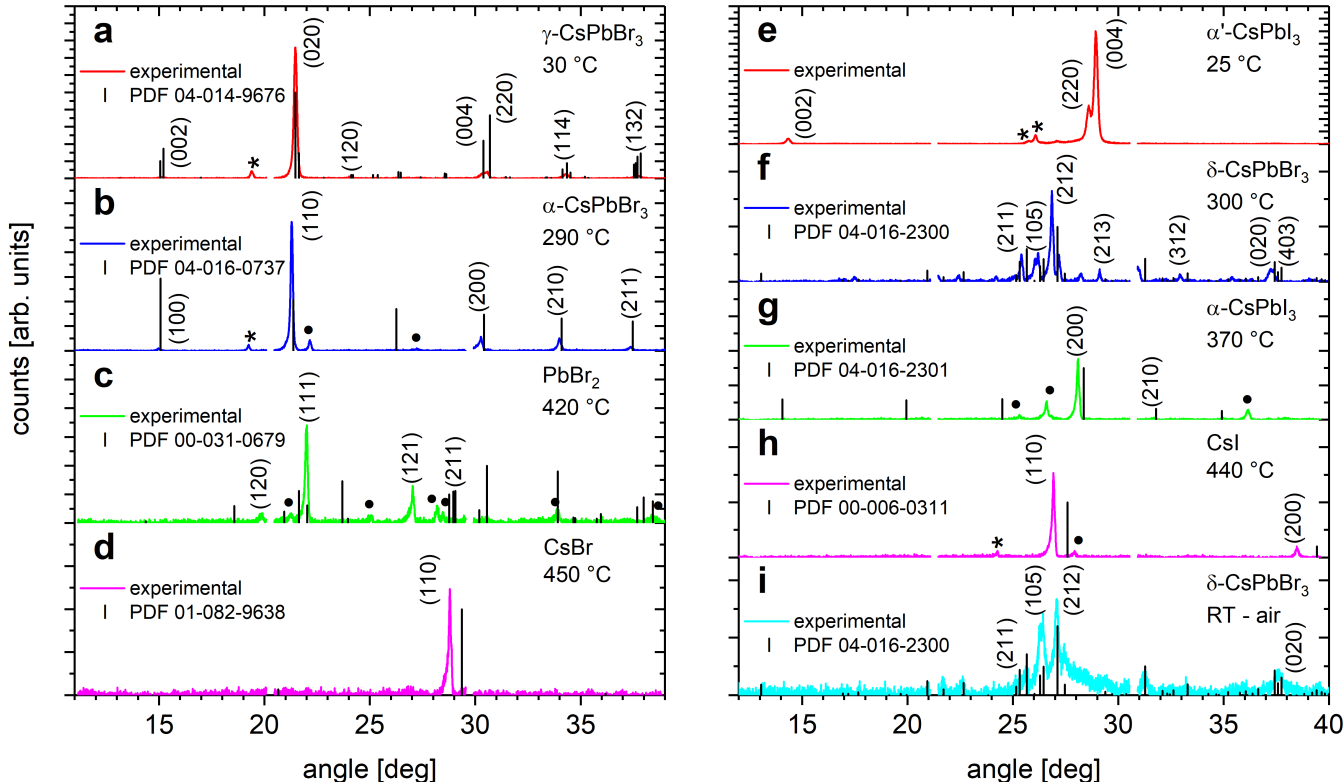
Figure 3: XRD diffractograms showing the materials seen in the experiments that are presented here. Peaks denoted with an asterisk are K_β peaks, peaks with a dot belong to a different material. The references are depicted as black bars.

A selection of XRD-scans that indicate particular materials and phases is compiled in figure 3. The scans shown are depicting γ-CsPbBr$_3$ (a), α-CsPbBr$_3$ (b), PbBr$_2$ (c), CsBr (d), α'-CsPbI$_3$ (e), δ-CsPbI$_3$ (f), α-CsPbI$_3$ (g), CsI (h) and δ-CsPbI$_3$ that was converted from the α'-phase under ambient air (i). The PbBr$_2$ scan shown in subfigure (c) corresponds to the reference data if this is shifted by about 1.75° to smaller angles, with the matching peaks being (111), (121), (211) and (120). This is a larger shift than what we would expect

10

due to thermal expansion alone. We tentatively suggest that the Cs might be partly still incoporated into the film, stretching the lattice and leading to the observed shift.

It is well known that the black α'-phase of $CsPbI_3$ is unstable in ambient air and that it will convert into the yellow δ-$CsPbI_3$-phase when exposed to it.[8,11,16] A black α'-$CsPbI_3$ film was grown at room temperature in vacuum and the chamber was subsequently flooded with N_2. The XRD pattern of the film remained unchanged and is displayed in figure 3 (e). This indicates at least partial stability of the black α'-$CsPbI_3$ under atmospheric nitrogen pressure. Subsequently, the chamber was flooded with air, which within seconds lead to a fast colour change from black to yellow, accompanied by a sudden shift in the LLS signal. The XRD pattern after this exposure corresponds to the yellow δ-phase and can be seen in figure 3 (i). A direct comparison of the XRD pattern before and after the phase transition can be found within the supporting information. These results highlight the fact that the phase transition is not solely driven by temperature but also depends significantly on the atmospheric conditions, most probably especially on the moisture level. These results therefore lend credence to the hypothesis that an influx of atmospheric water into the crystal matrix acts as a catalyst for the observed phase transition, as is suggested by Ahmad et al.[12]

Preliminary tests suggest that the stability of the black $CsPbI_3$ phase to ambient air exposure might be enhanced by mixing with Br. However, for conclusive results further experiments are needed. Stabilisation by mixing I-Br ions has also been reported for example by Sutton et al.[26]

The thermal expansion coefficients of $CsPbBr_3$ and δ-$CsPbI_3$ have been determined by observing the shift of the XRD peaks. The relation between the distance of the lattice plains d and the corresponding XRD peak angle 2θ can be described by Bragg's law. d is calculated as follows:

$$d = \frac{\lambda}{2 \cdot \sin(2\theta)}. \tag{1}$$

The thermal expansion of a given lattice constant a is then expressed with the help of the
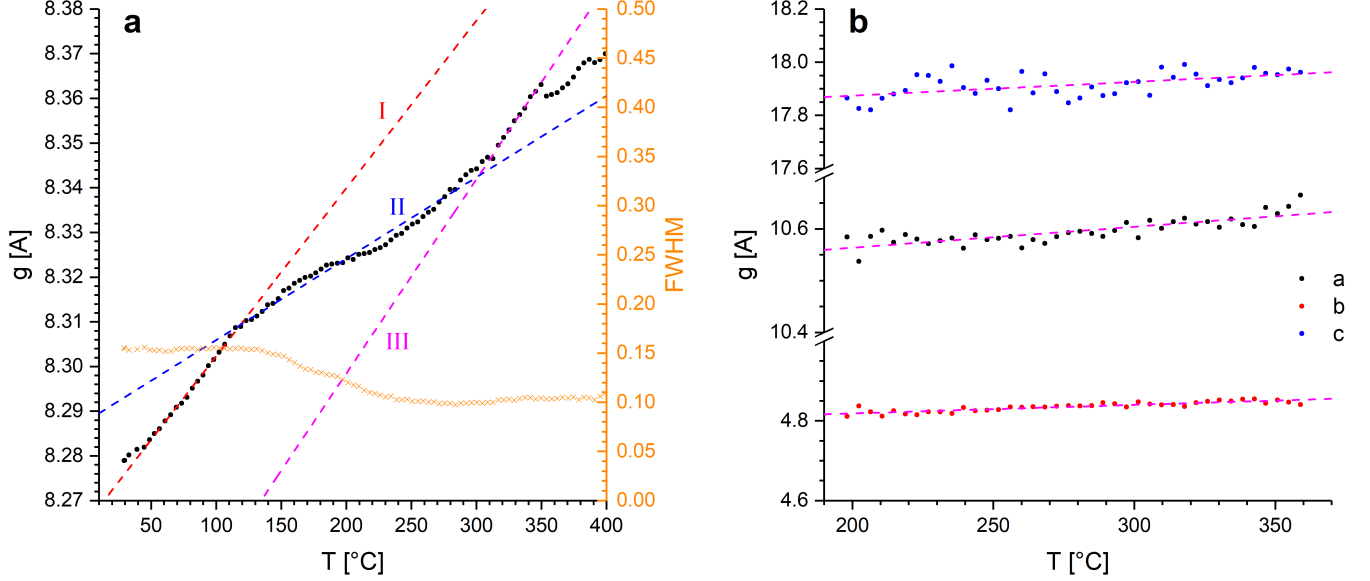
Figure 4: (a) shows the relation between the lattice plain distance of the (020) plains of $CsPbBr_3$ and the temperature T. The FWHM of the (020) peak is also shown. (b) shows this relation for the three lattice constants a, b and c of the orthorhombic δ-$CsPbI_3$.

linear thermal expansion coefficient α:

$$a = a_0 \cdot (1 + \alpha \cdot \Delta T). \tag{2}$$

Here ΔT is the temperature difference and a_0 is the lattice constant at $\Delta T = 0$. A linear fit of a over the temperature difference ΔT with the form $y = x_0 + m \cdot x$ yields $m = a_0 \cdot \alpha$ as the slope with $x_0 = a_0$. The given uncertainties were calculated from the errors of the fit by gaußian error propagation.

From the development of the lattice plain distance of the $CsPbBr_3$, three distinct stages can be discerned. The expansion coefficient has been determined separately for the three sections, using the peak at the position that corresponds to the (020) lattice plains in the orthorhombic phase. The expansion coefficient for section I, which reaches up to $115\,^{\circ}\mathrm{C}$, was determined to be $\alpha_I = (45.4 \pm 0.6) \cdot 10^{-6}\,\mathrm{K}^{-1}$, for section II, reaching up to $315\,^{\circ}\mathrm{C}$, $\alpha_{II} = (22.0 \pm 0.5) \cdot 10^{-6}\,\mathrm{K}^{-1}$ and for section III $\alpha_{III} = (52.9 \pm 1.5) \cdot 10^{-6}\,\mathrm{K}^{-1}$. Rodova et al. reported average linear expansion coefficients of $\alpha = 45 \cdot 10^{-6}\,\mathrm{K}^{-1}$ for temperatures

12

below 85 °C, $\alpha = 38 \cdot 10^{-6} \, \mathrm{K}^{-1}$ between 93 °C and 124 °C and $\alpha = 33 \cdot 10^{-6} \, \mathrm{K}^{-1}$ from 140 °C to 230 °C.[13] The results for section I lie in good agreement with the expansion coefficient proposed by Rodova et al. for the low temperature range. The FWHM seen in figure 4 (a) indicates a transition during section II. This section might be subject to additional distortions induced by the occurrence of $PbBr_2$ secondary phases. The high temperature section III exceeds the temperature range examined by Rodova et al. The linear thermal expansion coefficient that was obtained for this section only slightly exceeds that of the low temperature section I.

During the existence of the α'-$CsPbI_3$-phase only the (002), (004) and (220) peak were visible, which provides only two linearly independent peaks, which is not sufficient for calculating the three lattice parameters of an orthorhombic lattice. To obtain the values for a, b and c of the orthorhombic δ-$CsPbI_3$ shown in figure 4 (c), the (212)-, (213)- and (312)-peaks were factored in. A linear fit of the lattice constants taken over the temperature yielded the values for the linear thermal expansion coefficients with $\alpha_a = (38.6 \pm 4.6) \cdot 10^{-6} \, \mathrm{K}^{-1}$, $\alpha_b = (44.9 \pm 4.1) \cdot 10^{-6} \, \mathrm{K}^{-1}$ and $\alpha_c = (29.1 \pm 7.6) \cdot 10^{-6} \, \mathrm{K}^{-1}$. Trots et al. propose a volumetric expansion coefficient of $\alpha_V = 11.8 \cdot 10^{-5} \, \mathrm{K}^{-1}$,[19] which is in good agreement with our findings, resulting in $\alpha_V = \alpha_a + \alpha_b + \alpha_c = 11.3 \cdot 10^{-5} \, \mathrm{K}^{-1}$.

These results show comparable linear expansion coefficients to the MA-based perovskites, where for $MAPbI_3$ the linear thermal expansion coefficient is $\alpha = 43.3 \cdot 10^{-6} \, \mathrm{K}^{-1}$ and for $MAPbBr_3$ $\alpha = 33.3 \cdot 10^{-6} \, \mathrm{K}^{-1}$ has been determined.[27]

Conclusions

In conclusion we present an upper limit for the thermal stability of $CsPbBr_3$ at 360 °C and of $CsPbI_3$ at 390 °C and showed that the decomposition, in contrast to the hybrid $MAPbX_3$ perovskites, is initiated by the sublimination of the respective materials' lead halide. The results imply that the thermal stability of Cs based perovskites is limited by the lead halide

component and significantly surpasses that of the MA based perovskites. Under vacuum conditions we find that $CsPbI_3$ crystallizes in a black, orthorhombic α'-crystal phase. Upon heating the film undergoes the phase transitions from a black, orthorhombic α'-phase to a yellow, orthorhombic δ-phase to a black, cubic α-phase.

XRD measurements confirm that black, orthorhombic α'-$CsPbI_3$ will convert immediately to yellow, orthorhombic δ-$CsPbI_3$ upon exposure to ambient air, underlining the instability of α-$CsPbI_3$ in ambient air. The linear thermal expansion coefficient of the (020) plain of $CsPbBr_3$ has been determined to be $\alpha_I = (45.4 \pm 0.6) \cdot 10^{-6}\,\mathrm{K}^{-1}$ for temperatures below $115\,°C$, $\alpha_{II} = (22.0 \pm 0.5) \cdot 10^{-6}\,\mathrm{K}^{-1}$ for temperatures below $315\,°C$ and $\alpha_{III} = (52.9 \pm 1.5) \cdot 10^{-6}\,\mathrm{K}^{-1}$ above $315\,°C$. For the three lattice constants of the orthorhombic δ-$CsPbI_3$ the linear thermal expansion coefficients have been determined to be $\alpha_a = (38.6 \pm 4.6) \cdot 10^{-6}\,\mathrm{K}^{-1}$, $\alpha_b = (44.9 \pm 4.1) \cdot 10^{-6}\,\mathrm{K}^{-1}$ and $\alpha_c = (29.1 \pm 7.6) \cdot 10^{-6}\,\mathrm{K}^{-1}$ respectively.

Acknowledgements

Conflicts of Interest

There are no conflicts of interest to disclose.

Supporting Information Available

Substrate cleaning procedure, evaporation temperatures, brand names of used materials, notes regarding the lead bromide X-ray absorption, comparison of $CsPbI_3$ under N_2 and air.

References

(1) Habisreutinger, S. N.; Leijtens, T.; Eperon, G. E.; Stranks, S. D.; Nicholas, R. J.; Snaith, H. J. Carbon Nanotube/Polymer Composites as a Highly Stable Hole Collection Layer in Perovskite Solar Cells. *Nano Letters* **2014**, *14*, 5561–5568.

(2) Beal, R. E.; Slotcavage, D. J.; Leijtens, T.; Bowring, A. R.; Belisle, R. A.; Nguyen, W. H.; Burkhard, G. F.; Hoke, E. T.; McGehee, M. D. Cesium Lead Halide Perovskites with Improved Stability for Tandem Solar Cells. *The Journal of Physical Chemistry Letters* **2016**, *7*, 746–751.

(3) Leguy, A. M. A.; Hu, Y.; Campoy-Quiles, M.; Alonso, M. I.; Weber, O. J.; Azarhoosh, P.; van Schilfgaarde, M.; Weller, M. T.; Bein, T.; Nelson, J. et al. Reversible Hydration of CH3NH3PbI3 in Films, Single Crystals, and Solar Cells. *Chemistry of Materials* **2015**, *27*, 3397–3407.

(4) Sheng, R.; Wen, X.; Huang, S.; Hao, X.; Chen, S.; Jiang, Y.; Deng, X.; Green, M. A.; Ho-Baillie, A. W. Y. Photoluminescence Characterisations of a Dynamic Aging Process of Organic–Inorganic CH3NH3PbBr3 Perovskite. *Nanoscale* **2016**, *8*, 1926–1931.

(5) Yang, J.; Siempelkamp, B. D.; Liu, D.; Kelly, T. L. Investigation of CH3NH3PbI3 Degradation Rates and Mechanisms in Controlled Humidity Environments Using in Situ Techniques. *ACS Nano* **2015**, *9*, 1955–1963.

(6) Kulbak, M.; Cahen, D.; Hodes, G. How Important is the Organic Part of Lead Halide Perovskite Photovoltaic Cells? Efficient CsPbBr3 Cells. *Journal of Physical Chemistry Letters* **2015**, *6*, 2452–2456.

(7) Kulbak, M.; Gupta, S.; Kedem, N.; Levine, I.; Bendikov, T.; Hodes, G.; Cahen, D. Cesium Enhances Long-Term Stability of Lead Bromide Perovskite-Based Solar Cells. *The Journal of Physical Chemistry Letters* **2015**, *7*, 167–172.

(8) Eperon, G. E.; Patern, G. M.; Sutton, R. J.; Zampetti, A.; Haghighirad, A. A.; Cacialli, F.; Snaith, H. J. Inorganic Caesium Lead Iodide Perovskite Solar Cells. *Journal Materials Chemistry A* **2015**, *3*, 19688–19695.

(9) Hutter, E. M.; Sutton, R. J.; Chandrashekar, S.; Abdi-Jalebi, M.; Stranks, S. D.; Snaith, H. J.; Savenije, T. J. Vapour-Deposited Cesium Lead Iodide Perovskites: Microsecond Charge Carrier Lifetimes and Enhanced Photovoltaic Performance. *ACS Energy Letters* **2017**, *2*, 1901–1908.

(10) Saliba, M.; Matsui, T.; Seo, J.-Y.; Domanski, K.; Correa-Baena, J.-P.; Nazeeruddin, M. K.; Zakeeruddin, S. M.; Tress, W.; Abate, A.; Hagfeldt, A. et al. Cesium-Containing Triple Cation Perovskite Solar Cells: Improved Stability, Reproducibility and High Efficiency. *Energy & Environmental Science* **2016**, *9*, 1989–1997.

(11) Chen, C.-Y.; Lin, H.-Y.; Chiang, K.-M.; Tsai, W.-L.; Huang, Y.-C.; Tsao, C.-S.; Lin, H.-W. All-Vacuum-Deposited Stoichiometrically Balanced Inorganic Cesium Lead Halide Perovskite Solar Cells with Stabilized Efficiency Exceeding 11%. *Advanced Materials* **2017**, *29*, 1605290.

(12) Ahmad, W.; Khan, J.; Niu, G.; Tang, J. Inorganic CsPbI3 Perovskite-Based Solar Cells: A Choice for a Tandem Device. *Solar RRL* **2017**, *1*, 1700048.

(13) Rodova, M.; Brozek, J.; Knizek, K.; Nitsch, K. Phase Transitions in Ternary Caesium Lead Bromide. *Journal of Thermal Analysis and Calorimetry* **2003**, *71*, 667–673.

(14) Stoumpos, C. C.; Malliakas, C. D.; Peters, J. A.; Liu, Z.; Sebastian, M.; Im, J.; Chasapis, T. C.; Wibowo, A. C.; Chung, D. Y.; Freeman, A. J. et al. Crystal Growth of the Perovskite Semiconductor CsPbBr3: A New Material for High-Energy Radiation Detection. *Crystal Growth & Design* **2013**, *13*, 2722–2727.

(15) Eperon, G. E.; Stranks, S. D.; Menelaou, C.; Johnston, M. B.; Herz, L. M.; Snaith, H. J.

Formamidinium Lead Trihalide: A Broadly Tunable Perovskite for Efficient Planar Heterojunction Solar Cells. *Energy & Environmental Science* **2014**, *7*, 982.

(16) Moller, C. K. Crystal Structure and Photoconductivity of Cæsium Plumbohalides. *Nature* **1958**, *182*, 1436–1436.

(17) Yunakova, O. N.; Miloslavskii, V. K.; Kovalenko, E. N. Exciton Absorption Spectrum of Thin CsPbI3 and Cs4PbI6 Films. *Optics and Spectroscopy* **2012**, *112*, 91–96.

(18) Lai, M.; Kong, Q.; Bischak, C. G.; Yu, Y.; Dou, L.; Eaton, S. W.; Ginsberg, N. S.; Yang, P. Structural, Optical, and Electrical Properties of Phase-Controlled Cesium Lead Iodide Nanowires. *Nano Research* **2017**, *10*, 1107–1114.

(19) Trots, D.; Myagkota, S. High-Temperature Structural Evolution of Caesium and Rubidium Triiodoplumbates. *Journal of Physics and Chemistry of Solids* **2008**, *69*, 2520–2526.

(20) Wang, C.; Chesman, A. S. R.; Jasieniak, J. J. Stabilizing the Cubic Perovskite Phase of CsPbI3 Nanocrystals by Using an Alkyl Phosphinic Acid. *Chemical Communications* **2017**, *53*, 232–235.

(21) Yi, C.; Luo, J.; Meloni, S.; Boziki, A.; Ashari-Astani, N.; Grtzel, C.; Zakeeruddin, S. M.; Rthlisberger, U.; Grtzel, M. Entropic Stabilization of Mixed A-Cation ABX3 Metal Halide Perovskites for High Performance Perovskite Solar Cells. *Energy & Environmental Science* **2016**, *9*, 656–662.

(22) Cola, M.; Massarotti, V.; Riccardi, R.; Sinistri, C. Binary Systems Formed by Lead Bromide with (Li, Na, K, Rb, Cs and Tl)Br: a DTA and Diffractometric Study. *Zeitschrift für Naturforschung A* **1971**, *26*.

(23) Dualeh, A.; Gao, P.; Seok, S. I.; Nazeeruddin, M. K.; Grtzel, M. Thermal Behavior of

Methylammonium Lead-Trihalide Perovskite Photovoltaic Light Harvesters. *Chemistry of Materials* **2014**, *26*, 6160–6164.

(24) Conings, B.; Drijkoningen, J.; Gauquelin, N.; Babayigit, A.; D'Haen, J.; D'Olieslaeger, L.; Ethirajan, A.; Verbeeck, J.; Manca, J.; Mosconi, E. et al. Intrinsic Thermal Instability of Methylammonium Lead Trihalide Perovskite. *Advanced Energy Materials* **2015**, *5*, 1500477.

(25) Pistor, P.; Burwig, T.; Brzuska, C.; Weber, B.; Frnzel, W. Thermal Stability and Miscibility of Co-Evaporated Methyl Ammonium Lead Halide (MAPbX3, X = I, Br, Cl) Thin Films Analysed by In Situ X-Ray Diffraction. *Journal of Materials Chemistry A* **2018**,

(26) Sutton, R. J.; Eperon, G. E.; Miranda, L.; Parrott, E. S.; Kamino, B. A.; Patel, J. B.; Hrantner, M. T.; Johnston, M. B.; Haghighirad, A. A.; Moore, D. T. et al. Bandgap-Tunable Cesium Lead Halide Perovskites with High Thermal Stability for Efficient Solar Cells. *Advanced Energy Materials* **2016**, *6*, 1502458.

(27) Rakita, Y.; Cohen, S. R.; Kedem, N. K.; Hodes, G.; Cahen, D. Mechanical Properties of APbX 3 (A = Cs or CH3NH3 X = I or Br) Perovskite Single Crystals. *MRS Communications* **2015**, *5*, 623–629.